

Reduced volatility of aerosols from surface emission to the top of planetary boundary layer

Quan Liu¹, Dantong Liu^{2,*}, Yangzhou Wu², Kai Bi³, Wenkang Gao⁴, Ping Tian³, Delong Zhao³, Siyuan Li², Chenjie Yu⁵, Guiqian Tang⁴, Yunfei Wu⁶, Kang Hu², Shuo Ding², Qian Gao³, Fei Wang³, Shaofei Kong⁷, Hui He^{3,8}, Mengyu Huang^{3,8}, Deping Ding³

¹ State Key Laboratory of Severe Weather & Key Laboratory of Atmospheric Chemistry of CMA, Chinese Academy of Meteorological Sciences, Beijing 100081, China

² Department of Atmospheric Sciences, School of Earth Sciences, Zhejiang University, Hangzhou, Zhejiang, 310027, China

10 ³ Beijing Weather Modification Office, Beijing 100089, China

⁴ State Key Laboratory of Atmospheric Boundary Layer Physics and Atmospheric Chemistry, Institute of Atmospheric Physics, Chinese Academy of Sciences, Beijing 100029, China

⁵ Centre for Atmospheric Sciences, School of Earth and Environmental Sciences, University of Manchester, Manchester M13 9PL, UK.

15 ⁶ Key Laboratory of Middle Atmosphere and Global Environment Observation (LAGEO), Institute of Atmospheric Physics, Chinese Academy of Sciences, Beijing 100029, China

⁷ Department of Atmospheric Science, School of Environmental Studies, China University of Geosciences, Wuhan, 430074, China

20 ⁸ Field experiment base of cloud and precipitation research in North China, China Meteorological Administration, Beijing, 101200, China

Correspondence to: Dantong Liu (dantongliu@zju.edu.cn)

Abstract. Aerosols from surface emission can be transported upwards through convective mixing in the planetary boundary layer (PBL), which subsequently interact with clouds, serving as important sources to nucleate droplets or ice particles. However, the evolution of aerosol composition during this vertical transport has yet to be explicitly understood. In this study, simultaneous measurements of detailed aerosol compositions were conducted at both sites, urban Beijing (50m a.s.l.) and HaiTuo mountain (1344m a.s.l.) during wintertime, representing the anthropogenically polluted surface environment and the top of the PBL respectively. The pollutants from surface emissions were observed to reach the mountain site on daily basis through daytime PBL convective mixing. From surface to the top of PBL, we found efficient transport or formation for lower-volatile species (black carbon, sulfate and low-volatile organic aerosol, OA); however notable reduction of semi-volatile

25
30

substances, such as the fractions of nitrate and semi-volatile OA reduced by 74% and 76% respectively, during the upward transport. This implied the mass loss of these semi-volatile species was driven by the evaporation process, which repartitioned the condensed semi-volatile substances to gas-phase, when aerosols were transported and exposed to a cleaner environment. **In combination** with the oxidation processes, these led to enhanced oxidation state of OA at the top of the PBL compared to surface environment, with an increase of oxygen to carbon atomic ratio by 0.2. Such reduction of aerosol volatility during vertical transport may be important in modifying its viscosity, nucleation activity and atmospheric lifetime.

1 Introduction

Substances in the atmosphere present as aerosol and gas **phases**, are subject to phase transformation during their lifetime (Pankow, 1994, 1987). **Gas-to-particle partition processes** thermodynamically determine the production of secondary aerosol mass and the constituents of gases **through condensation or evaporation process. The condensation process leads** to gas molecular partitioning to the condensed phase, **while** the evaporation process occurs when aerosols were diluted in an environment with lower concentration (Donahue et al., 2006). Hereby their physiochemical properties could be modified, such as the condensation results in enlarging aerosol size (Riipinen et al., 2011; Riipinen et al., 2012) or production of new particle (Zhang et al., 2004; Kulmala et al., 2013); the evaporation led to loss of particulate mass (May et al., 2015; Cubison et al., 2011). These have important impacts in altering the radiative interactions of aerosols, by changing the mass of aerosols hereby the direct radiative impacts (Tsigaridis et al., 2014; Wang et al., 2014), or in the number concentration and the ability of cloud condensation nuclei for the indirect radiative impacts (D'Andrea et al., 2013; Kuang et al., 2009). The repartitioned gases from aerosols during dilution could experience chemical evolution and further contribute to the modification of aerosol properties (Zhang et al., 2007; Robinson et al., 2007).

In regions with intense anthropogenic activities, such as megacities, nitrate and sulfate are dominant inorganic aerosol chemical components due to intensive emissions of gaseous precursors (anthropogenic NO_x and SO_2) with secondary formation through photochemical and heterogenous/aqueous reactions (Zhang et al., 2015; Huang et al., 2014; Guo et al., 2014; Sun et al., 2016). Although the formation mechanisms of secondary inorganic aerosol are relatively well understood, OA processing in atmospheric transport process remains poorly characterized (Shrivastava et al., 2017). Organic compounds are ubiquitous in ambient aerosol with a large contribution (20-90%) to submicron aerosol mass loadings, including primary OA (POA) and secondary OA (SOA) (Zhang et al., 2007). During atmospheric aging processes, OA physiochemical properties, such as

60 volatility, hygroscopicity, viscosity, and oxidation state, have been significantly transformed. For example, semi-volatile organic materials are repartitioned to gas phase when ambient vapor partial pressure is lower than that in particle phase, and then those vapors can be further photo-oxidized and produce SOA with lower volatility (Robinson et al., 2007). In addition, SOA tend to dominate the OA mass along with atmospheric aging processes, which modulate OA properties to be more oxidized and hygroscopic (Jimenez et al., 2009).

65 The vertical transport of aerosol and gases in the PBL from surface to the lower free troposphere (FT) importantly determines the influence of anthropogenic emissions to the upper level of the atmosphere, e.g. aerosols at the upper level of the PBL may have more important feedback effects in influencing the boundary layer dynamics (Li et al., 2017). The aerosol could be upward transported from surface to upper level through daytime convective mixing in the PBL (Garratt, 1994). Previous studies have used aircraft (Liu et al., 2020b; Zhao et al., 2019) or balloon platform (Ran et al., 2016; Li et al., 2015) to in-situ measure the vertical profiles of PBL, however lack of sufficient temporal coverage nor full chemical components. The evolution of aerosol properties during this vertical transport in the PBL on daily-basis **has not been** fully understood. In this study, simultaneous and continuous measurements of detailed aerosol compositions were performed at both surface and surface-influenced mountain sites **using advanced instrumentations, which provides an opportunity to realize the**
75 **high time-resolution variations at different altitudes. Relative location of the mountain site to the top of the PBL varies with diurnal variation of PBL height (PBLH), which leave the mountain site in the free troposphere most time of the day and being influenced by PBL air masses around midday. Through comparing the difference of aerosol chemical compositions between the two sites,** we aim to investigate the modification of compositions during the upward transport in the PBL and explore the generic mechanisms in driving the evolution of chemical
80 composition.

2 Experimental and methods

2.1 Experimental sites

Simultaneous measurements of detailed aerosol compositions (organics, nitrate, sulfate, ammonium, chloride, and black carbon) and gaseous pollutants (NO_x , SO_2 , CO , O_3) were conducted during January 6th to 22th, 2019 at both
85 surface and surface-influenced mountain sites, representing the anthropogenically polluted surface urban environment and the top of the PBL respectively. All aerosol measurements were performed downstream of a $\text{PM}_{2.5}$ impactor (BGI Inc.) at both sites, and dried by a Nafion tube before splitting to the sample inlets of instruments.

Figure 1a shows the locations of surface and mountain sites, and the spatial distribution of mean aerosol optical depth during the observation period. The surface site locates in the Institute of Atmospheric Physics, Chinese Academy of Science (IAP, 39.97°N, 116.37°E, 50m a.s.l.), which represents the urban environment in Beijing influenced by intense surface anthropogenic emissions, such as local traffic and cooking emissions (Sun et al., 2016; Zhang et al., 2014). The mountain site (Haituo mountain, 40.52°N, 115.78°E, 1344 m a.s.l.) locates in the northwest Beijing area with a straight-line distance of ~85 km from Beijing downtown. The Haituo mountain belongs to Taihang mountains and connects to the continental plateau extended to the west. The surroundings of this site are covered with broad-leaf forest and without distinct anthropogenic emissions except for a few villages at the foot of the mountain. Thus, it can be considered an ideal receptor site for regional transport influenced and/or local influenced by vertical transport under certain conditions.

2.2 Instrumentation and data analysis

Non-refractory aerosol chemical components including nitrate (NO₃), sulfate (SO₄), ammonium (NH₄), chloride (Chl) and organics (Org) were measured by the high-resolution time-of-flight aerosol mass spectrometer (HR-ToF-AMS, Aerodyne Research Inc.) at each site. The applied collection efficiency (CE) for the AMS measurement at the surface and mountain site was shown in Fig. S1, following the principle by Middlebrook et al. (2012). Ionization efficiency (IE) calibrations were performed by using size-selected (300nm) ammonium nitrate particles, and default relative IE (RIE) values were used for Org (1.4), NO₃ (1.1), SO₄ (1.2), NH₄ (4.0) and Chl (1.3). The IE calibration was conducted before and after experiment at both sites.

Standard AMS data analysis software packages (SQUIRREL 1.59D and PIKA 1.19D) were used to deconvolve mass spectrum and obtain mass concentrations of chemical components. Then, high-resolution mass spectra of OA for m/z 12-150 at both sites were analyzed by the positive matrix factorization (PMF) with PMF2.exe algorithm (Paatero and Tapper, 1994), following the data-processing and factors-selecting steps given by Ulbrich et al. (2009) and Zhang et al. (2011). As a result, five factors were resolved from the surface OA, including three primary OA (POA), that is, hydrocarbon-like OA (HOA) from traffic emissions, cooking-related OA (COA), and coal combustion OA (CCOA), and two secondary OA (SOA), that is, semi-volatile oxidized OA (SV-OOA) and low-volatility oxygenated OA (LV-OOA). Note that the COA factor was not resolved from the mountain OA, which has been frequently reported in urban environments (Zhang et al., 2011). The other four analogous factors were also resolved from the mountain OA. Detailed diagnostic plots of the PMF results are presented in Fig. S2 and S3, while the PMF-derived mass spectra and time series of organic components at both sites are shown in Fig. S4 and S5. Elemental ratios including oxygen-to-carbon (O/C) and hydrogen-to-carbon (H/C) were determined

from analysis of high-resolution mass spectra of OA based on the improved-ambient (I-A) method (Canagaratna
120 et al., 2015). While the elemental ratios were also calculated using the Aiken-ambient (A-A) method (Aiken et al.,
2008) for comparison with previous studies. The elemental ratios reported in this study are obtained from the I-A
method unless otherwise stated.

Black carbon (BC) mass was measured by a single particle soot photometer (SP2, DMT Inc.), following the
calibration and data analysis processes by Liu et al. (2020). Gaseous pollutants (i.e. NO_x, SO₂, CO, and O₃) were
125 measured by gas analyzers (model 42i, 43i, 48i, and 49i, Thermo Scientific Inc.). The PBLH was determined by
an enhanced single-lens lidar ceilometer (CL51, Vaisala Co.), using the retrieval method by Tang et al. (2015).
Meteorology variables (RH and temperature) were measured using WXT-510 (Vaisala Co.).

2.3 Air mass history

Three-dimensional air mass histories were calculated by the Numerical Atmospheric dispersion Modeling
130 Environment (NAME) (Jones et al., 2007), which is a lagrangian dispersion model following 3D trajectories of
plume parcels by Monte Carlo methods. The meteorological data source uses the global configuration of UK Met
Office's Unified Model. In order to calculate the historical air mass contribution, the model release tracer
particles at a nominal rate of 1 g s⁻¹, with a maximum travel time of 24 hours in backward mode from target site
(i.e. Haituo mountain site in this study), and the integrated time was recorded on a 0.25 ° × 0.25 ° horizontal grid
135 from 0 to 1000 m above the ground, aggregating over all particles for a given release period. In this study, the
potential source contribution of particles to the mountain site (back to 24 hours) from air masses classified as four
main regions (Fig. 1b): Local (39-41.5°N, 115-117°E, a square region around central Beijing covering both
measurement sites), West (32-41.5°N, 104-115°E), North (41.5-45°N, 104-121°E), and South (32-39 °N, 115-
121°E). Figure 1b presents a typical example of westerly dominated air mass from NAME outputs. The particle
140 flux is integrated in each segregated region, and contributions of each air mass fractions could be obtained.

3 Results and discussions

3.1 Upward transport of aerosols around midday

We aim to classify the source influences on the mountain site from the local surface emission or wider regional
area. Air mass history analysis showed pronounced diurnal pattern of local air mass influence (as determined by
145 the NAME dispersion model), peaking around midday (11:00-14:00). The local air mass fraction as calculated
from the dispersion model is only used to indicate the predominant local air mass influence in the midday. The

aerosol concentration contained in the air mass depends on the transport efficiency, reaction and deposition rate of each aerosol type. The fraction of transported aerosols, even for the inert BC may not be quantitatively comparable with the air mass fraction. The maximum local influence was consistent with the most developed PBLH (Fig. 1c). This suggested the strongest influence of surface emissions to the mountain through midday convective mixing (CM) hereby termed as CM period. For certain period (Jan. 9th to 12th), westerly air mass continuously influenced the mountain site (grey bar in Fig. 1d-h), which advected regional pollutants from the polluted high plateau, adding on the persistent local emission, termed as regional advection (RA) period. Note that the RA period was also influenced by the convective mixing of surface sources around midday, however being combined with additional sources from other regions besides the surface emission. In this study, the statistical results of the RA period include the whole period marked in the grey bar in Fig. 1d-h, and the rest period is used for the statistics of CM period.

Figure 2 gives the statistical diurnal variations of aerosol species during CM and RA periods respectively, with species of BC, OA, nitrate, sulfate shown in Fig. 2a-d, and PMF-derived organic components in Fig. 2e-h. During CM period, the chemically-inert species such as BC, showed clear diurnal pattern on the mountain, with elevated concentration by 82% (from 0.19 to 0.34 $\mu\text{g m}^{-3}$) from midday to early afternoon (Fig. 2a). This pattern was highly consistent with the development of PBLH and local air mass contribution. On the surface, the diurnal variation of BC concentration showed a minimum at the same hours due to the dilution effect of developed PBL, but had a sharp enhancement during nighttime due to the accumulation in the shallow nighttime PBL. Notably, BC concentration at 11:00-14:00 on the mountain almost matched with that on the surface, suggesting the well mixed layer because of the daytime convective mixing. The inert gas CO was also efficiently transported without significant loss from surface to mountain (Fig. S6c). This means the pollutants, if without reactions, evaporation or other forms of losses, were able to be efficiently transported upwards from surface to the mountain site through the daytime convective mixing.

3.2 Loss of semi-volatile particulate mass from surface to mountain

Aerosol chemical compositions showed remarkable differences between both sites even when PBL fully developed (Fig. 3), i.e. nitrate (23%) and organics (54%) dominated at surface, while sulfate (23%) and organics (45%) dominated at the top of PBL. Meanwhile, the characteristics of OA varied from POA-dominated (59%) to SOA-dominated (64%). Statistical analysis in Fig. 4 highlights the difference between both sites during the periods of CM midday (11:00-14:00), CM night (23:00-02:00) and RA, where CM midday represents the period with the most efficient convective mixing. The matched concentrations of BC and CO between surface and

mountain demonstrated the capability of boundary layer in transporting pollutants upwards in terms of atmospheric dynamics. For other species such as organics and nitrate, there was still an enhancement on the mountain peaking around midday, however the loadings was 61% and 74% lower than the surface at the same hours (Fig. 2b,c, Fig. 4a), which contrasted with the efficient transport of BC. The low-volatile species sulfate at both sites showed no apparent (or only broad) diurnal pattern and matched concentration in the midday, consistent with its gas precursor SO₂ (Fig. S6b), indicating their regional feature and the aerosol production was not sufficiently rapid to display notable diurnal variation.

The diurnal patterns of all PMF-resolved organic components on the mountain presented a midday peak feature at different amplitude (Fig. 2e-h), suggesting there was no additional source around the site, and the upward transport processes for these components was affected by various factors. Previous studies found POA (e.g. HOA and CCOA) has substantial semi-volatile materials and presents relatively high volatility (Cao et al., 2018). The comparison between the two sites showed significantly decreased semi-volatile species (i.e. HOA, CCOA and SV-OOA), their concentrations on the mountain were significantly lower than that at surface by 48%, 24% and 76% in the CM midday, respectively (Fig. 4a-b). The LV-OOA is a typical SOA which predominantly exists in aged air mass (Zhang et al., 2011). In contrast with semi-volatile species, the low volatile LV-OOA on the mountain showed a poorly defined diurnal pattern and its concentrations in the midday were higher than that at surface by 52%, which maybe partially caused by further oxidation of relative fresh species in vertical transport process.

The results above demonstrated that during vertical transport, the loss of particulate masses only occurred for semi-volatile substances (nitrate, POA and SV-OOA), but not for low-volatile species (BC, LV-OOA, sulfate) or inert gas (CO). Meanwhile, these losses had occurred in a relatively dry condition without notable wet scavenging (Fig. S7b). Due to few anthropogenic emissions on the mountain, the concentrations of gaseous precursors, such as ammonia and nitric acid vapor etc., should be significantly lower than that in urban environment. This suggested that the evaporation process may have played an important role in repartitioning the condensed phase rich of semi-volatile species to gas phase, which occurred when the activity of semi-volatile species in condensed phase (molar fraction multiplied by activity coefficient) was higher than the partial vapor pressure (relative to equilibrium vapor pressure of pure substance under certain temperature) (Pankow, 1994, 1987). Given the wintertime for the experiment, the mean temperature shifted from -5.5 to 3.8 °C from surface to mountain in the CM midday (Fig. S7a), which was already sufficiently low for even the most volatile species (i.e. ammonium nitrate) to be in condensed phase (Salo et al., 2011) at both sites. Therefore, the temperature decrease within this low range had not driven appreciable condensation process, but the reduction of ambient

concentration at mountain (given no additional sources but only contributed by surface emission) was the main reason leading to the evaporation. A previous study basing on aircraft measurements in this region showed that, aerosol chemical composition had a significant variation from surface to the top of the PBL under high RH conditions (surface RH>60%), which caused by secondary formation through the enhanced aqueous/heterogeneous processes in vertical direction (Liu et al., 2020). However, the RH was quite low at both sites (most of time RH<40%, Fig. S7b), below the deliquescence RH for most substances (Cruz and Pandis, 2000), water vapor may thus had not importantly participated in the phase transformation or chemical reactions during vertical transport. In addition, the bulk equilibrium between gas and condensed phase may be significantly hindered under conditions of lower temperature and lower RH due to the kinetically limited diffusion rate at the aerosol surface (Koop et al., 2011). Therefore, the viscosity of aerosols may be enhanced and OA may be present as semi-solid or glassy state under these conditions. This means the evaporation process may be eventually depressed, when aerosols are transported from lower and moister boundary layer to the upper level with lower temperature and moisture, hereby aerosols may be more solid-like and resistant to the evaporation. This evaporation-dominated variation on aerosol composition from the surface to the top of the PBL tend to only occur at the cold and dry condition.

This evaporation process tended to occur along the path of vertical transport, with higher loss rate when larger gradient of concentration between in condensed phase and ambient air (Donahue et al., 2006;Shrivastava et al., 2006;Robinson et al., 2007). Previous studies pointed the dilution could be particularly important for biomass burning emissions (Li et al., 2021). The high concentrations of condensed phase could importantly contribute to the gaseous precursors, and under certain conditions, could form secondary aerosol. In addition, these low-volatile aerosols transported to the free troposphere may have longer lifetime and be transported to a longer distance (Liu et al., 2020a). Here we only observed the resultant compositions after being transported to the top of PBL, but at which atmospheric layer this process had mostly occurred remained inconclusive. There may be some production process, e.g. photochemical oxidation around midday, which contributed to some increase of SV-OOA concentration around midday (Fig. 2g). The overall reduced SV-OOA suggested its net loss, which was evaporation prevailed production processes, during upwards transport.

During CM night, pollutants (except O₃) were mostly accumulated at surface (Fig. 4c) due to local emissions and secondary formation processes occurred in a shallow nighttime PBL and interruption of vertical transport to high layers. Note that, the diurnal variation of surface O₃ showed a significant reduction at night due to rapid consumption by strong NO titration, in contrast with a maintainable high O₃ concentration on the mountain without apparent diurnal pattern (Fig. S6d). For RA period, due to the additional input of pollutants from a wider

regional region besides the local influence, the diurnal variation at mountain was diminished, but showed
240 enhanced concentrations at all hours (Fig. 2), indicated that robust regional advection process also significantly
affects aerosol concentration and variation at high layer. Because the surface site was more influenced by local
sources, most species had higher concentrations at surface than mountain, apart from sulfur compounds (SO₂ and
sulfate, in Fig. 4d). This implies the possible high-level sulfuric sources, e.g. emissions from industrial stack
directly emitting into a higher level in the PBL (Wu et al., 2018; Xu et al., 2014).

245 3.3 Modification on the oxidation state of OA

The Van Krevelen-triangle (VK) diagram (Fig. 5a) could indicate the likely oxidation pathway of OA by
investigating different degrees of changes on the oxygen or hydrogen over carbon element ratio, depending on
the way of adding functional groups (Van Krevelen, 1950). For example, the replacement of a hydrogen atom
with an alcohol/peroxide group (-OH, -OOH) results in a slope of 0, while the replacement of a hydrogen atom
250 with a carboxylic acid group (-COOH) results in a slope of -1 without fragmentation (C-C bond breaking), and
-0.5 with fragmentation (Ng et al., 2010). Results mapping on the H:C versus O:C atomic ratio showed
discernible regimes between both sites (Fig. 5a). The surface O:C varied at 0.16-0.75, with an average of
0.42±0.09 (0.33±0.08 with A-A method), generally consistent with those (0.29-0.41, A-A method) previously
reported in Beijing (Xu et al., 2015; Zhang et al., 2014; Sun et al., 2016). Mountain OA showed significantly
255 higher O:C (varied at 0.39 to 0.96, with an average of 0.62±0.07) and lower H:C (1.23-1.64) than surface, similar
with the regime of LV-OOA dominated periods observed in Rocky Mountain National Park (~2740m a.s.l.)
(Schurman et al., 2015). Here the surface (slope=-0.64) showed a steeper slope than mountain (slope=-0.33). The
surface thus tended to be dominated by the oxidation pathway of -COOH addition (without fragmentation), which
showed an apparent decrease of H/C. However, the OA at mountain tended to be oxidized in mix with
260 alcohol/peroxide and -COOH addition (with fragmentation) pathway, hereby less decrease on H/C.

Difference of m/z spectra for each PMF factor between surface and mountain was analyzed to further investigate
the chemical modification of OA from each source (Fig. 6). The mountain CO₂⁺ fraction in m/z spectra of all
PMF factors enhanced at various extents, indicating the oxidation by adding carboxyl groups (Ng et al., 2011).
For HOA and SV-OOA, a range of hydrocarbon fragments decreased at mountain (Fig. 6a, c), which tended to be
265 consistent with the evaporation mechanism proposed in section 3.2 that semi-volatile species may have been
repartitioned to the gas phase when transported to the mountain, and these evaporated species may contain
significant fraction of more volatile hydrocarbons (Cappa and Jimenez, 2010). Note that the diurnal variation of
mountain O:C characterized by slightly fluctuating at a high value region, in contrast with a distinct peak in the

early afternoon appearing in the diurnal variation of surface O:C (Fig. 5b). This implied there was no additional
270 primary emissions on the mountain to contribute either particles or VOCs. Meanwhile, mountain O₃
concentration maintained at a high level without apparent diurnal pattern, in contrast with prominent diurnal
variation of surface O₃ (Fig. S6d). The maintainable high O₃ concentration on the mountain meant a high
oxidation capability. Thus the repartitioned gas species during upwards transport, in addition to the directly
275 transported VOCs, may be further oxidized by the high level of O₃ throughout the day and night, and re-
condensed on particle phase (Robinson et al., 2007). The continuous oxidation on these vapors potentially
contributed to production of SOA, which may partly explain the higher levels of O:C at mountain than surface
throughout all hours. The mass spectra of mountain HOA and SV-OOA had substantial reductions mainly at ion
series C_xH_{2x-1}⁺ (Fig. 6a,c), suggesting the O₃ oxidation may occur on unsaturated bonds (e.g. alkenes) (Paulson
and Orlando, 1996), hereby following a less steep slope on the VK space, consistent with above.
280 For CCOA and LV-OOA, H:C had a substantial decrease but O:C only increased slightly (Fig. 6b, d). The m/z
difference of CCOA shows substantial decrease of C_xH_yO⁺ fragments at mountain, which may compensate some
of the O:C increase. Some C_xH_y⁺ fragments showed increase at mountain, which tended to be consistent with the
view that the CCOA is largely contributed by non-local sources (Li et al., 2019). This factor may have not
experienced significant vertical transport from the surface, thus showing some fresher signatures (the C_xH_y⁺
285 fragments) at mountain. LV-OOA had a large enhancement of CHO⁺ and reduction of CH₂O⁺, maybe caused by
some transformation of alcohols to carbonyl compounds (Grosjean et al., 1993).

4 Conclusions and implications

The increase of oxidation state could be caused by the evaporation process by losing the less oxidized and more
volatile species, and the evaporated gases could be further oxidized to partition to a more oxidized phase. The
290 evaporative loss had occurred in a relatively short time scale, i.e. a few hours' vertical transported induced by
daytime convective mixing of boundary layer, as reflected by 76% decrease of semi-volatile organic masses, and
74% of nitrate. These losses had occurred in a relatively dry condition without notable wet scavenging, therefore
the evaporative loss tended to dominate. For the other period on the mountain rather than midday, there was
additional primary sources in contributing neither particles nor VOCs, thus most of the vapors repartitioned from
295 the condensed phase in the midday may stay and be subjected to oxidation at the mountain. These continuous
inputs of gases to the top of boundary layers on daily basis serve a source of precursors to be oxidized and
contribute to an important fraction of highly oxidized SOA.

All of these processes lead to a consistent manner in enhancing the oxidation state of OA at the top of PBL, which may modify the hygroscopicity and viscosity of OA (Koop et al., 2011). Combining with the more efficiently transported less-volatile species, these processes consistently led to overall decreased volatility of aerosols at top of the PBL, where cloud formation is initialized, influencing the activities of both cloud condensation nuclei and ice nuclei. **These lower-volatile aerosols could be transported to a longer distance in the free troposphere hereby having longer lifetime.** This also implies that the aerosol characteristics at surface may not represent that at upper levels, where the evolution during transport should be considered in evaluating the contribution of surface emissions to cloud particle nucleation and their atmospheric lifetime.

Data availability. All data in this paper are available from the authors upon request (liuquan620@126.com).

Author contributions. DD, MH, and HH led and designed the study. QL, DL, YW, KB, WG, PT, DZ, SL, CY, TG, YW, KH, SD, QG, FW and SK were involved in collecting, processing and analysis of surface and mountain data. QL and DL carried out the data analysis and wrote the paper. QL and all authors contributed to the discussions.

Competing interests. The authors declare that they have no conflict of interest.

Acknowledgments. This work was supported by National Key Research and Development Program of China (No. 2016YFA0602001, 2019YFC0214703), the National Natural Science Foundation of China (No. 41975177, 41875167), and the Beijing Natural Science Foundation (No. 8192021).

References

- Aiken, A. C., DeCarlo, P. F., Kroll, J. H., Worsnop, D. R., Huffman, J. A., Docherty, K. S., Ulbrich, I. M., Mohr, C., Kimmel, J. R., Sueper, D., Sun, Y., Zhang, Q., Trimborn, A., Northway, M., Ziemann, P. J., Canagaratna, M. R., Onasch, T. B., Alfarra, M. R., Prevot, A. S. H., Dommen, J., Duplissy, J., Metzger, A., Baltensperger, U., and Jimenez, J. L.: O/C and OM/OC Ratios of Primary, Secondary, and Ambient Organic Aerosols with High-Resolution Time-of-Flight Aerosol Mass Spectrometry, *Environ. Sci. Technol.*, 42, 4478-4485, 10.1021/es703009q, 2008.
- Canagaratna, M. R., Jimenez, J. L., Kroll, J. H., Chen, Q., Kessler, S. H., Massoli, P., Hildebrandt Ruiz, L., Fortner, E., Williams, L. R., Wilson, K. R., Surratt, J. D., Donahue, N. M., Jayne, J. T., and Worsnop, D. R.: Elemental ratio

- measurements of organic compounds using aerosol mass spectrometry: characterization, improved calibration, and implications, *Atmos. Chem. Phys.*, 15, 253-272, 10.5194/acp-15-253-2015, 2015.
- 330 Cao, L. M., Huang, X. F., Li, Y. Y., Hu, M., and He, L. Y.: Volatility measurement of atmospheric submicron aerosols in an urban atmosphere in southern China, *Atmos. Chem. Phys.*, 18, 1729-1743, 10.5194/acp-18-1729-2018, 2018.
- Cappa, C. D., and Jimenez, J. L.: Quantitative estimates of the volatility of ambient organic aerosol, *Atmos. Chem. Phys.*, 10, 5409-5424, 10.5194/acp-10-5409-2010, 2010.
- Cruz, C., and Pandis, S.: Deliquescence and Hygroscopic Growth of Mixed Inorganic–Organic Atmospheric Aerosol, 335 *Environ. Sci. Technol.*, 34, 4313-4319, 10.1021/es9907109, 2000.
- Cubison, M. J., Ortega, A. M., Hayes, P. L., Farmer, D. K., Day, D., Lechner, M. J., Brune, W. H., Apel, E., Diskin, G. S., Fisher, J. A., Fuelberg, H. E., Hecobian, A., Knapp, D. J., Mikoviny, T., Riemer, D., Sachse, G. W., Sessions, W., Weber, R. J., Weinheimer, A. J., Wisthaler, A., and Jimenez, J. L.: Effects of aging on organic aerosol from open biomass burning smoke in aircraft and laboratory studies, *Atmos. Chem. Phys.*, 11, 12049-12064, 10.5194/acp-11-12049-2011, 2011.
- 340 D'Andrea, S. D., Häkkinen, S. A. K., Westervelt, D. M., Kuang, C., Levin, E. J. T., Kanawade, V. P., Leaitch, W. R., Spracklen, D. V., Riipinen, I., and Pierce, J. R.: Understanding global secondary organic aerosol amount and size-resolved condensational behavior, *Atmos. Chem. Phys.*, 13, 11519-11534, 10.5194/acp-13-11519-2013, 2013.
- Donahue, N., Robinson, A., Stanier, C., and Pandis, S.: Coupled partitioning, dilution, and chemical aging of semivolatile organics, *Environ. Sci. Technol.*, 40, 2635-2643, 2006.
- 345 Garratt, J. R.: Review: the atmospheric boundary layer, *Earth Sci. Rev.*, 37, 89-134, 1994.
- Grosjean, D., Grosjean, E., and Williams, E. L.: Atmospheric chemistry of unsaturated alcohols, *Environ. Sci. Technol.*, 27, 2478-2485, 10.1021/es00048a026, 1993.
- Guo, S., Hu, M., Zamora, M. L., Peng, J., Shang, D., Zheng, J., Du, Z., Wu, Z., Shao, M., Zeng, L., Molina, M. J., and Zhang, R.: Elucidating severe urban haze formation in China, *Proceedings of the National Academy of Sciences of the United States* 350 *of America*, 111, 17373-17378, 10.1073/pnas.1419604111, 2014.
- Huang, R.-J., Zhang, Y., Bozzetti, C., Ho, K.-F., Cao, J.-J., Han, Y., Daellenbach, K. R., Slowik, J. G., Platt, S. M., Canonaco, F., Zotter, P., Wolf, R., Pieber, S. M., Bruns, E. A., Crippa, M., Ciarelli, G., Piazzalunga, A., Schwikowski, M., Abbaszade, G., Schnelle-Kreis, J., Zimmermann, R., An, Z., Szidat, S., Baltensperger, U., Haddad, I. E., and Prevot, A. S. H.: High secondary aerosol contribution to particulate pollution during haze events in China, *Nature*, 514, 218-222, 355 10.1038/nature13774, 2014.
- Jimenez, J. L., Canagaratna, M. R., Donahue, N. M., Prevot, A. S. H., Zhang, Q., Kroll, J. H., DeCarlo, P. F., Allan, J. D., Coe, H., Ng, N. L., Aiken, A. C., Docherty, K. S., Ulbrich, I. M., Grieshop, A. P., Robinson, A. L., Duplissy, J., Smith, J. D., Wilson, K. R., Lanz, V. A., Hueglin, C., Sun, Y. L., Tian, J., Laaksonen, A., Raatikainen, T., Rautiainen, J., Vaattovaara, P., Ehn, M., Kulmala, M., Tomlinson, J. M., Collins, D. R., Cubison, M. J., E., Dunlea, J., Huffman, J. A., Onasch, T. B., 360 Alfara, M. R., Williams, P. I., Bower, K., Kondo, Y., Schneider, J., Drewnick, F., Borrmann, S., Weimer, S., Demerjian, K., Salcedo, D., Cottrell, L., Griffin, R., Takami, A., Miyoshi, T., Hatakeyama, S., Shimono, A., Sun, J. Y., Zhang, Y. M.,

- Dzepina, K., Kimmel, J. R., Sueper, D., Jayne, J. T., Herndon, S. C., Trimborn, A. M., Williams, L. R., Wood, E. C., Middlebrook, A. M., Kolb, C. E., Baltensperger, U., and Worsnop, D. R.: Evolution of Organic Aerosols in the Atmosphere, *Science*, 326, 1525-1529, 10.1126/science.1180353, 2009.
- 365 Jones, A., Thomson, D., Hort, M., and Devenish, B.: The U.K. Met Office's Next-Generation Atmospheric Dispersion Model, NAME III, Air Pollution Modeling and Its Application XVII, Boston, MA, 2007, 580-589.
- Koop, T., Bookhold, J., Shiraiwa, M., and Pöschl, U.: Glass transition and phase state of organic compounds: dependency on molecular properties and implications for secondary organic aerosols in the atmosphere, *Phys. Chem. Chem. Phys.*, 13, 19238-19255, 10.1039/C1CP22617G, 2011.
- 370 Kuang, C., McMurry, P. H., and McCormick, A. V.: Determination of cloud condensation nuclei production from measured new particle formation events, *Geophys. Res. Lett.*, 36, 2009.
- Kulmala, M., Kontkanen, J., Junninen, H., Lehtipalo, K., Manninen, H. E., Nieminen, T., Petäjä, T., Sipilä, M., Schobesberger, S., and Rantala, P.: Direct observations of atmospheric aerosol nucleation, *Science*, 339, 943-946, 2013.
- Li, H., Cheng, J., Zhang, Q., Zheng, B., Zhang, Y., Zheng, G., and He, K.: Rapid transition in winter aerosol composition in
375 Beijing from 2014 to 2017: response to clean air actions, *Atmos. Chem. Phys.*, 19, 11485-11499, 10.5194/acp-19-11485-2019, 2019.
- Li, J., Fu, Q., Huo, J., Wang, D., Yang, W., Bian, Q., Duan, Y., Zhang, Y., Pan, J., Lin, Y., Huang, K., Bai, Z., Wang, S.-H., Fu, J. S., and Louie, P. K. K.: Tethered balloon-based black carbon profiles within the lower troposphere of Shanghai in the 2013 East China smog, *Atmos. Environ.*, 123, 327-338, <https://doi.org/10.1016/j.atmosenv.2015.08.096>, 2015.
- 380 Li, S., Liu, D., Hu, D., Kong, S., Wu, Y., Ding, S., Cheng, Y., Qiu, H., Zheng, S., Yan, Q., Zheng, H., Hu, K., Zhang, J., Zhao, D., Liu, Q., Sheng, J., Ye, J., He, H., and Ding, D.: Evolution of Organic Aerosol From Wood Smoke Influenced by Burning Phase and Solar Radiation, 126, e2021JD034534, <https://doi.org/10.1029/2021JD034534>, 2021.
- Li, Z., Guo, J., Ding, A., Liao, H., Liu, J., Sun, Y., Wang, T., Xue, H., Zhang, H., and Zhu, B.: Aerosol and boundary-layer interactions and impact on air quality, *Natl. Sci. Rev.*, 4, 810-833, 10.1093/nsr/nwx117, 2017.
- 385 Liu, D., Hu, K., Zhao, D., Ding, S., Wu, Y., Zhou, C., Yu, C., Tian, P., Liu, Q., Bi, K., Wu, Y., Hu, B., Ji, D., Kong, S., Ouyang, B., He, H., Huang, M., and Ding, D.: Efficient Vertical Transport of Black Carbon in the Planetary Boundary Layer, *Geophys. Res. Lett.*, 47, e2020GL088858, 10.1029/2020gl088858, 2020a.
- Liu, Q., Liu, D., Gao, Q., Tian, P., Wang, F., Zhao, D., Bi, K., Wu, Y., Ding, S., Hu, K., Zhang, J., Ding, D., and Zhao, C.:
390 Vertical characteristics of aerosol hygroscopicity and impacts on optical properties over the North China Plain during winter, *Atmos. Chem. Phys.*, 20, 3931-3944, 10.5194/acp-20-3931-2020, 2020b.
- May, A., Lee, T., McMeeking, G., Akagi, S., Sullivan, A., Urbanski, S., Yokelson, R., and Kreidenweis, S.: Observations and analysis of organic aerosol evolution in some prescribed fire smoke plumes, *Atmos. Chem. Phys.*, 15, 6323-6335, 2015.
- Ng, N. L., Canagaratna, M. R., Zhang, Q., Jimenez, J. L., Tian, J., Ulbrich, I. M., Kroll, J. H., Docherty, K. S., Chhabra, P. S., Bahreini, R., Murphy, S. M., Seinfeld, J. H., Hildebrandt, L., Donahue, N. M., DeCarlo, P. F., Lanz, V. A., Prévôt, A. S. H.,

- 395 Dinar, E., Rudich, Y., and Worsnop, D. R.: Organic aerosol components observed in Northern Hemispheric datasets from Aerosol Mass Spectrometry, *Atmos. Chem. Phys.*, 10, 4625-4641, 10.5194/acp-10-4625-2010, 2010.
- Ng, N. L., Canagaratna, M. R., Jimenez, J. L., Chhabra, P. S., Seinfeld, J. H., and Worsnop, D. R.: Changes in organic aerosol composition with aging inferred from aerosol mass spectra, *Atmos. Chem. Phys.*, 11, 6465-6474, 10.5194/acp-11-6465-2011, 2011.
- 400 Pankow, J. F.: Review and comparative analysis of the theories on partitioning between the gas and aerosol particulate phases in the atmosphere, *Atmos. Environ.*, 21, 2275-2283, 1987.
- Pankow, J. F.: An absorption model of gas/particle partitioning of organic compounds in the atmosphere, *Atmos. Environ.*, 28, 185-188, 1994.
- Paulson, S. E., and Orlando, J. J.: The reactions of ozone with alkenes: An important source of HOx in the boundary layer, *Geophys. Res. Lett.*, 23, 3727-3730, <https://doi.org/10.1029/96GL03477>, 1996.
- 405 Ran, L., Deng, Z., Xu, X., Yan, P., Lin, W., Wang, Y., Tian, P., Wang, P., Pan, W., and Lu, D.: Vertical profiles of black carbon measured by a micro-aethalometer in summer in the North China Plain, *Atmos. Chem. Phys.*, 16, 10441-10454, 10.5194/acp-16-10441-2016, 2016.
- Riipinen, I., Pierce, J. R., Yli-Juuti, T., Nieminen, T., Häkkinen, S., Ehn, M., Junninen, H., Lehtipalo, K., Petäjä, T., Slowik, J., Chang, R., Shantz, N. C., Abbatt, J., Leaitch, W. R., Kerminen, V. M., Worsnop, D. R., Pandis, S. N., Donahue, N. M., and Kulmala, M.: Organic condensation: a vital link connecting aerosol formation to cloud condensation nuclei (CCN) concentrations, *Atmos. Chem. Phys.*, 11, 3865-3878, 10.5194/acp-11-3865-2011, 2011.
- 410 Riipinen, I., Yli-Juuti, T., Pierce, J. R., Petäjä, T., Worsnop, D. R., Kulmala, M., and Donahue, N. M.: The contribution of organics to atmospheric nanoparticle growth, *Nat. Geosci.*, 5, 453-458, 10.1038/ngeo1499, 2012.
- 415 Robinson, A., Donahue, N., Shrivastava, M., Weitkamp, E., Sage, M., Grieshop, A., Lane, T., Pierce, J., and Pandis, S.: Rethinking Organic Aerosols: Semivolatile Emissions and Photochemical Aging, *Science*, 315, 1259-1262, 10.1126/science.1133061, 2007.
- Salo, K., Westerlund, J., Andersson, P. U., Nielsen, C., D'Anna, B., and Hallquist, M.: Thermal Characterization of Aminium Nitrate Nanoparticles, *J. PHYS. CHEM. A*, 115, 11671-11677, 10.1021/jp204957k, 2011.
- 420 Schurman, M. I., Lee, T., Sun, Y., Schichtel, B. A., Kreidenweis, S. M., and Collett Jr, J. L.: Investigating types and sources of organic aerosol in Rocky Mountain National Park using aerosol mass spectrometry, *Atmos. Chem. Phys.*, 15, 737-752, 10.5194/acp-15-737-2015, 2015.
- Shrivastava, M., Cappa, C. D., Fan, J., Goldstein, A. H., Guenther, A. B., Jimenez, J. L., Kuang, C., Laskin, A., Martin, S. T., Ng, N. L., Petaja, T., Pierce, J. R., Rasch, P. J., Roldin, P., Seinfeld, J. H., Shilling, J., Smith, J. N., Thornton, J. A.,
- 425 Volkamer, R., Wang, J., Worsnop, D. R., Zaveri, R. A., Zelenyuk, A., and Zhang, Q.: Recent advances in understanding secondary organic aerosol: Implications for global climate forcing, *Rev. Geophys.*, 55, 509-559, 10.1002/2016rg000540, 2017.

- Shrivastava, M. K., Lipsky, E. M., Stanier, C. O., and Robinson, A. L.: Modeling Semivolatile Organic Aerosol Mass Emissions from Combustion Systems, *Environ. Sci. Technol.*, 40, 2671-2677, 10.1021/es0522231, 2006.
- 430 Sun, Y., Du, W., Fu, P., Wang, Q., Li, J., Ge, X., Zhang, Q., Zhu, C., Ren, L., Xu, W., Zhao, J., Han, T., Worsnop, D. R., and Wang, Z.: Primary and secondary aerosols in Beijing in winter: sources, variations and processes, *Atmos. Chem. Phys.*, 16, 8309-8329, 10.5194/acp-16-8309-2016, 2016.
- Tang, G., Zhu, X., Hu, B., Xin, J., Wang, L., Munkel, C., Mao, G., and Wang, Y.: Impact of emission controls on air quality in Beijing during APEC 2014: lidar ceilometer observations, *Atmos. Chem. Phys.*, 15, 12667-12680, 10.5194/acp-15-12667-435 2015, 2015.
- Tsigrakis, K., Daskalakis, N., Kanakidou, M., Adams, P., Artaxo, P., Bahadur, R., Balkanski, Y., Bauer, S., Bellouin, N., and Benedetti, A.: The AeroCom evaluation and intercomparison of organic aerosol in global models, *Atmos. Chem. Phys.*, 14, 10845-10895, 2014.
- Ulbrich, I. M., Canagaratna, M. R., Zhang, Q., Worsnop, D. R., and Jimenez, J. L.: Interpretation of organic components 440 from Positive Matrix Factorization of aerosol mass spectrometric data, *Atmos. Chem. Phys.*, 9, 2891-2918, 10.5194/acp-9-2891-2009, 2009.
- Van Krevelen, D. W.: Graphical-statistical method for the study of structure and reaction processes of coal, *Fuel*, 24, 269-284, 1950.
- Wang, X., Heald, C., Ridley, D., Schwarz, J., Spackman, J., Perring, A., Coe, H., Liu, D., and Clarke, A.: Exploiting 445 simultaneous observational constraints on mass and absorption to estimate the global direct radiative forcing of black carbon and brown carbon, *Atmos. Chem. Phys.*, 14, 10989-11010, 2014.
- Wu, F., Xie, P., Li, A., Mou, F., Chen, H., Zhu, Y., Zhu, T., Liu, J., and Liu, W.: Investigations of temporal and spatial distribution of precursors SO₂ and NO₂ vertical columns in the North China Plain using mobile DOAS, *Atmos. Chem. Phys.*, 18, 1535-1554, 10.5194/acp-18-1535-2018, 2018.
- 450 Xu, W. Q., Sun, Y. L., Chen, C., Du, W., Han, T. T., Wang, Q. Q., Fu, P. Q., Wang, Z. F., Zhao, X. J., Zhou, L. B., Ji, D. S., Wang, P. C., and Worsnop, D. R.: Aerosol composition, oxidation properties, and sources in Beijing: results from the 2014 Asia-Pacific Economic Cooperation summit study, *Atmos. Chem. Phys.*, 15, 13681-13698, 10.5194/acp-15-13681-2015, 2015.
- Xu, W. Y., Zhao, C. S., Ran, L., Lin, W. L., Yan, P., and Xu, X. B.: SO₂ noontime-peak phenomenon in the North China 455 Plain, *Atmos. Chem. Phys.*, 14, 7757-7768, 10.5194/acp-14-7757-2014, 2014.
- Zhang, J. K., Sun, Y., Liu, Z. R., Ji, D. S., Hu, B., Liu, Q., and Wang, Y. S.: Characterization of submicron aerosols during a month of serious pollution in Beijing, 2013, *Atmos. Chem. Phys.*, 14, 2887-2903, 10.5194/acp-14-2887-2014, 2014.
- Zhang, Q., Jimenez, J. L., Canagaratna, M. R., Allan, J. D., Coe, H., Ulbrich, I., Alfarra, M. R., Takami, A., Middlebrook, A. M., Sun, Y. L., Dzepina, K., Dunlea, E., Docherty, K., DeCarlo, P. F., Salcedo, D., Onasch, T., Jayne, J. T., Miyoshi, T., 460 Shimono, A., Hatakeyama, S., Takegawa, N., Kondo, Y., Schneider, J., Drewnick, F., Borrmann, S., Weimer, S., Demerjian, K., Williams, P., Bower, K., Bahreini, R., Cottrell, L., Griffin, R. J., Rautiainen, J., Sun, J. Y., Zhang, Y. M., and Worsnop,

- D. R.: Ubiquity and dominance of oxygenated species in organic aerosols in anthropogenically-influenced Northern Hemisphere midlatitudes, *Geophys. Res. Lett.*, 34, L13801, 10.1029/2007gl029979, 2007.
- 465 Zhang, Q., Jimenez, J., Canagaratna, M., Ulbrich, I., Ng, N., Worsnop, D., and Sun, Y.: Understanding atmospheric organic aerosols via factor analysis of aerosol mass spectrometry: a review, *Anal. Bioanal. Chem.*, 401, 3045-3067, 10.1007/s00216-011-5355-y, 2011.
- Zhang, R., Suh, I., Zhao, J., Zhang, D., Fortner, E. C., Tie, X., Molina, L. T., and Molina, M. J.: Atmospheric New Particle Formation Enhanced by Organic Acids, *Science*, 304, 1487-1490, 10.1126/science.1095139 %J Science, 2004.
- 470 Zhang, X. Y., Wang, J. Z., Wang, Y. Q., Liu, H. L., Sun, J. Y., and Zhang, Y. M.: Changes in chemical components of aerosol particles in different haze regions in China from 2006 to 2013 and contribution of meteorological factors, *Atmos. Chem. Phys.*, 15, 12935-12952, 10.5194/acp-15-12935-2015, 2015.
- Zhao, D., Huang, M., Tian, P., He, H., Lowe, D., Zhou, W., Sheng, J., Wang, F., Bi, K., Kong, S., Yang, Y., Liu, Q., Liu, D., and Ding, D.: Vertical characteristics of black carbon physical properties over Beijing region in warm and cold seasons, *Atmos. Environ.*, 213, 296-310, <https://doi.org/10.1016/j.atmosenv.2019.06.007>, 2019.

475

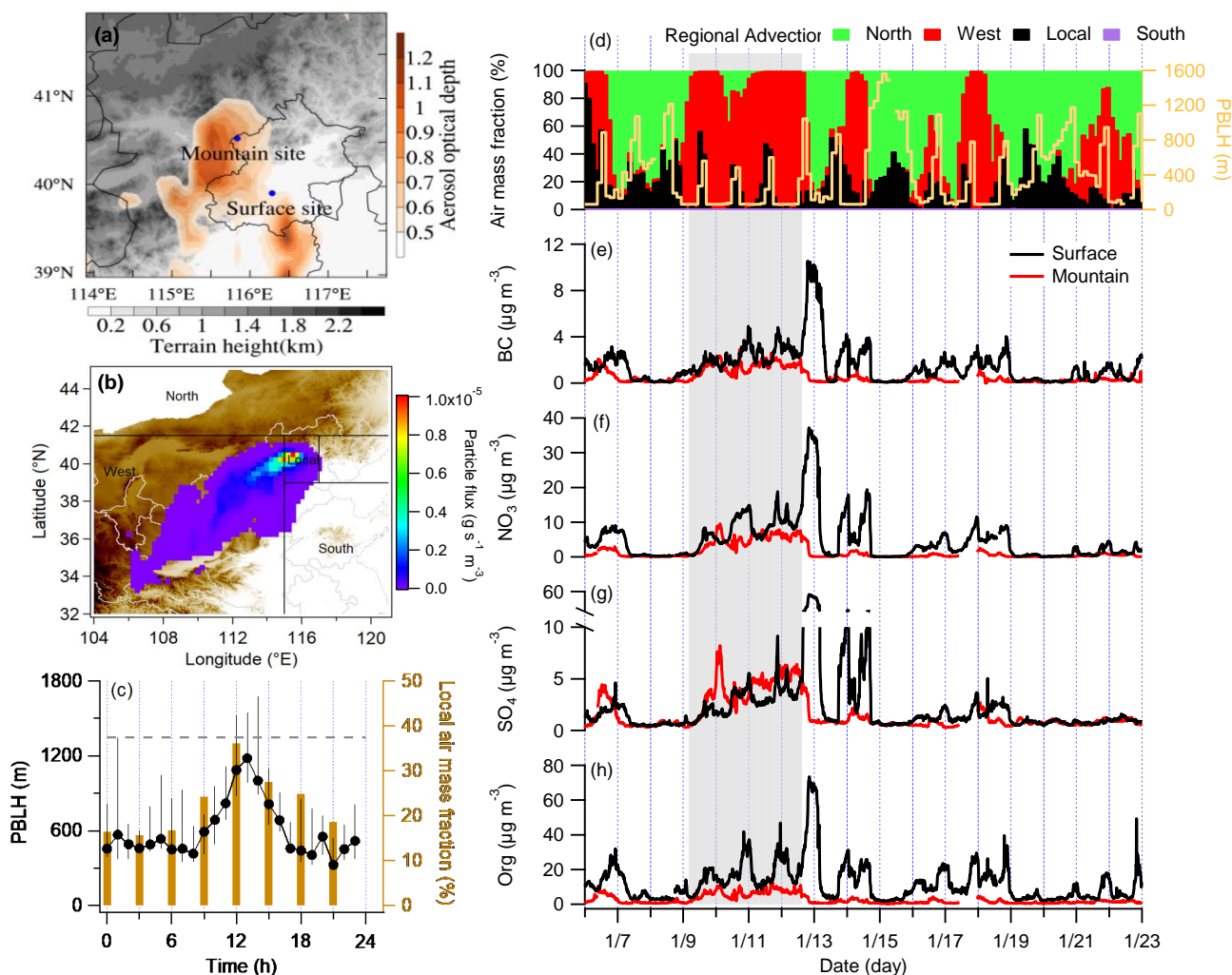


Fig. 1. Experimental overview. (a) spatial distribution of mean aerosol optical depth for the experimental month, with locations of surface and mountain sites, colored by terrain height; (b) a typical example of westerly dominated air mass from the NAME dispersion model outputs; (c) diurnal cycles of the planetary boundary layer height (PBLH) and local air mass fraction contributed to the mountain site during the experimental period, with whiskers showing the 25th and 75th percentiles, and the dash line denote the altitude of the mountain site; (d) time series of air mass fractions at the mountain and PBLH; (e-h) time series of black carbon (BC), nitrate (NO₃), sulfate (SO₄), and organics (Org), with the black and red lines showing the surface and mountain site respectively.

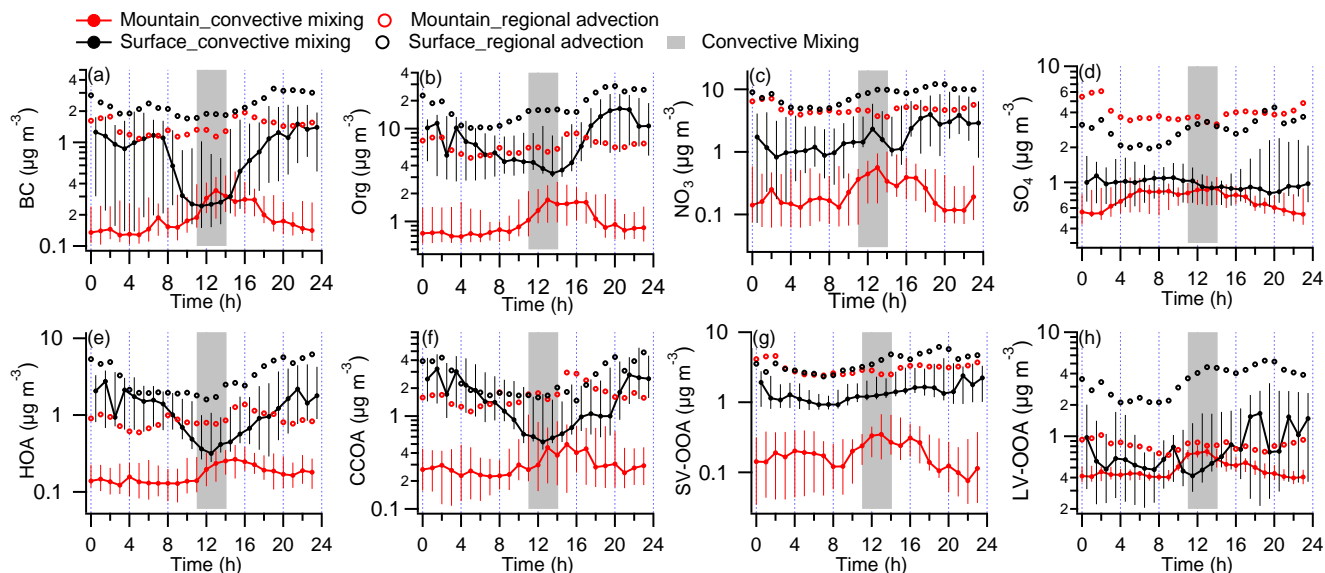


Fig. 2. Diurnal variations of key aerosol compositions at both sites during convective mixing (CM) and regional advection (RA) periods, (a) black carbon (BC); (b) organics (Org); (c) nitrate (NO_3); (d) sulfate (SO_4); (e) the sum of hydrocarbon OA (HOA) and cooking related OA (COA); (f) coal combustion-related OA (CCOA); (g) semi-volatile oxygenated OA (SV-OOA); (h) low-volatile oxygenated OA (LV-OOA). The black and red colors represent the surface and mountain site respectively. Solid circles and error bars show the median, 75th, and 25th percentiles in CM period. Circle markers show the mean value in RA period. Grey bar represents the time in the day (11:00-14:00) with the most developed PBL.

495

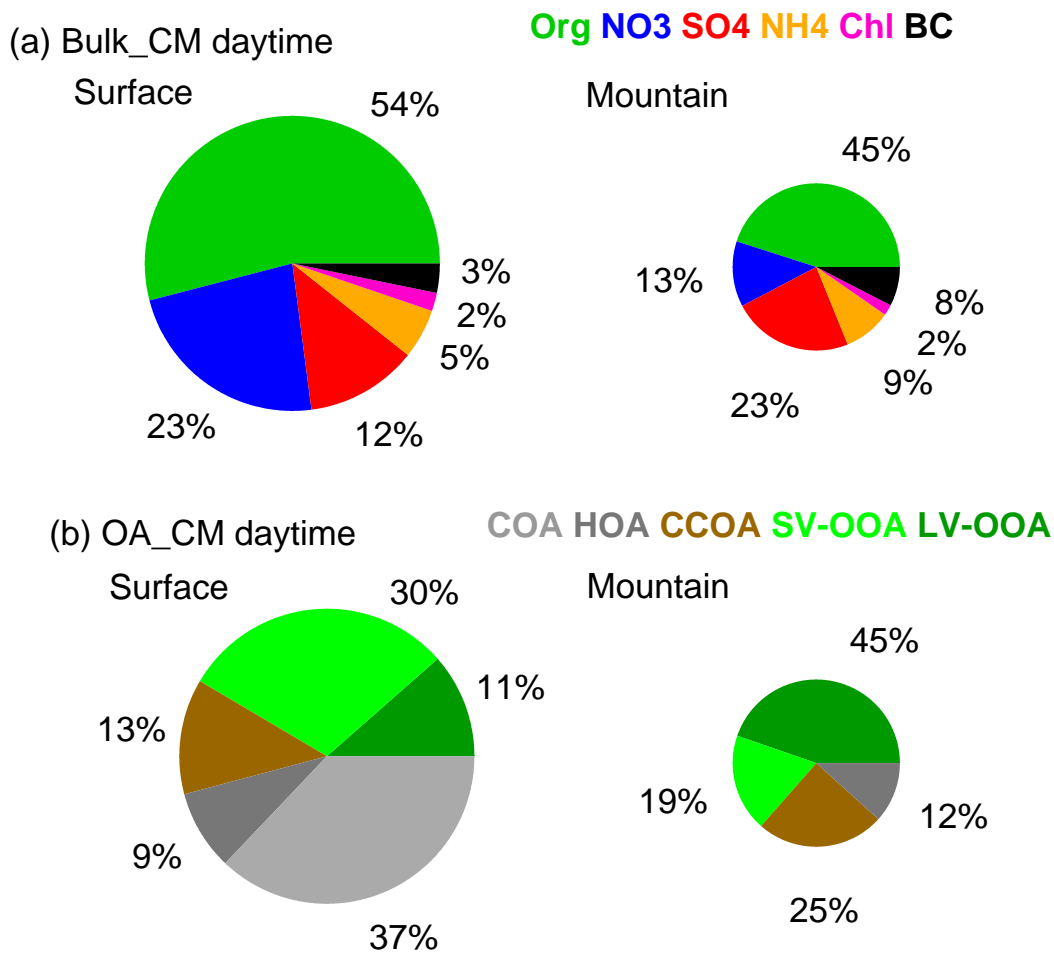
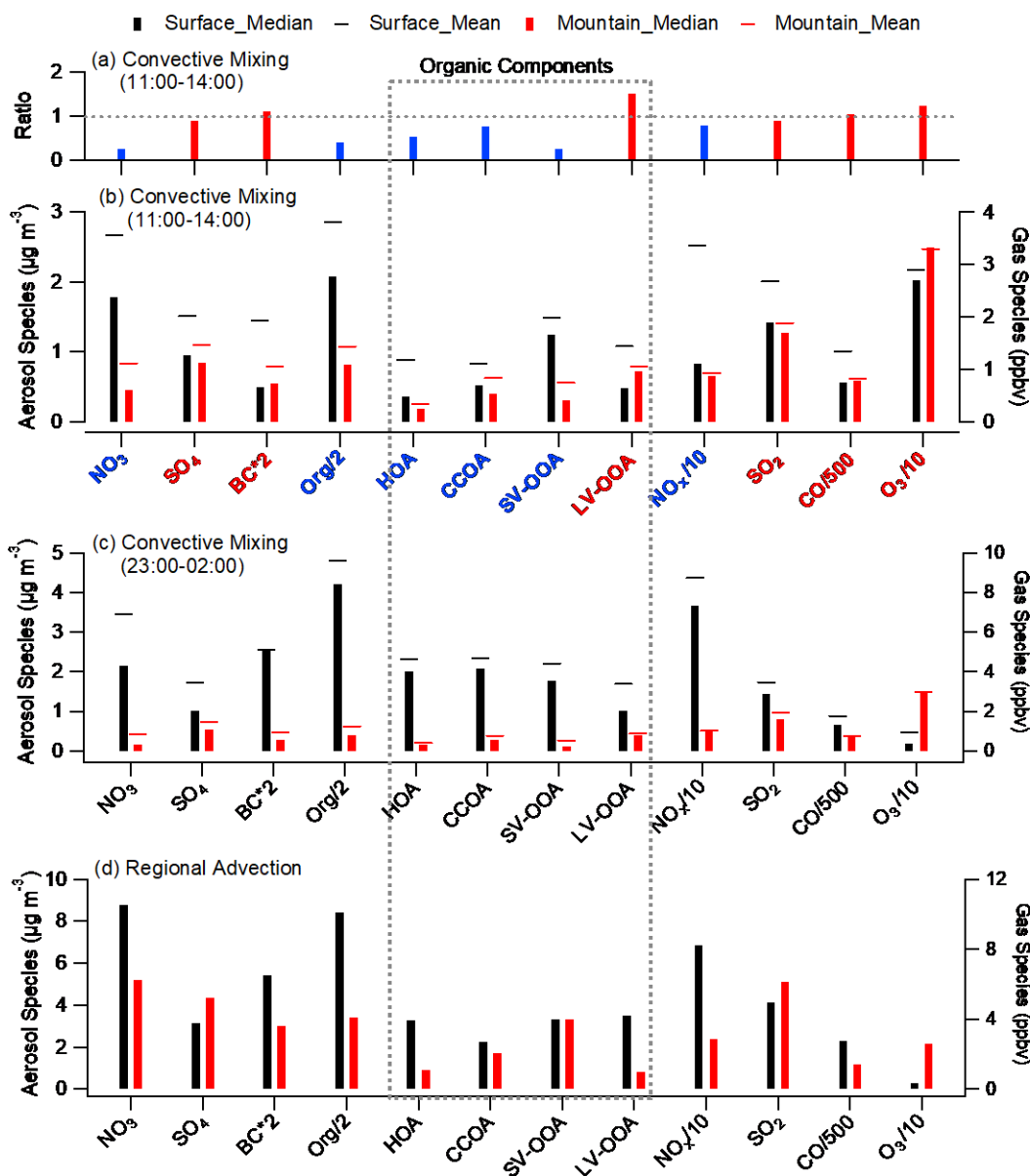


Fig. 3. Averaged chemical composition at both sites during convective mixing (CM) period daytime (11:00-14:00), (a) bulk aerosols; (b) organic aerosols.



505 **Fig. 4.** Statistical analysis of chemical components at both sites. (a) the mountain over surface ratio of key species during convective mixing (CM) period daytime (11:00-14:00); (b) median concentrations of key species during CM daytime, with black and red bars denoting the surface and mountain respectively and the cap showing the mean; (c-d) The same with panel b) but for the periods of CM night and RA period. Species with mountain/surface ratio above and below 0.8 (the transport efficiency for BC and CO) are marked in red and blue, respectively.

510

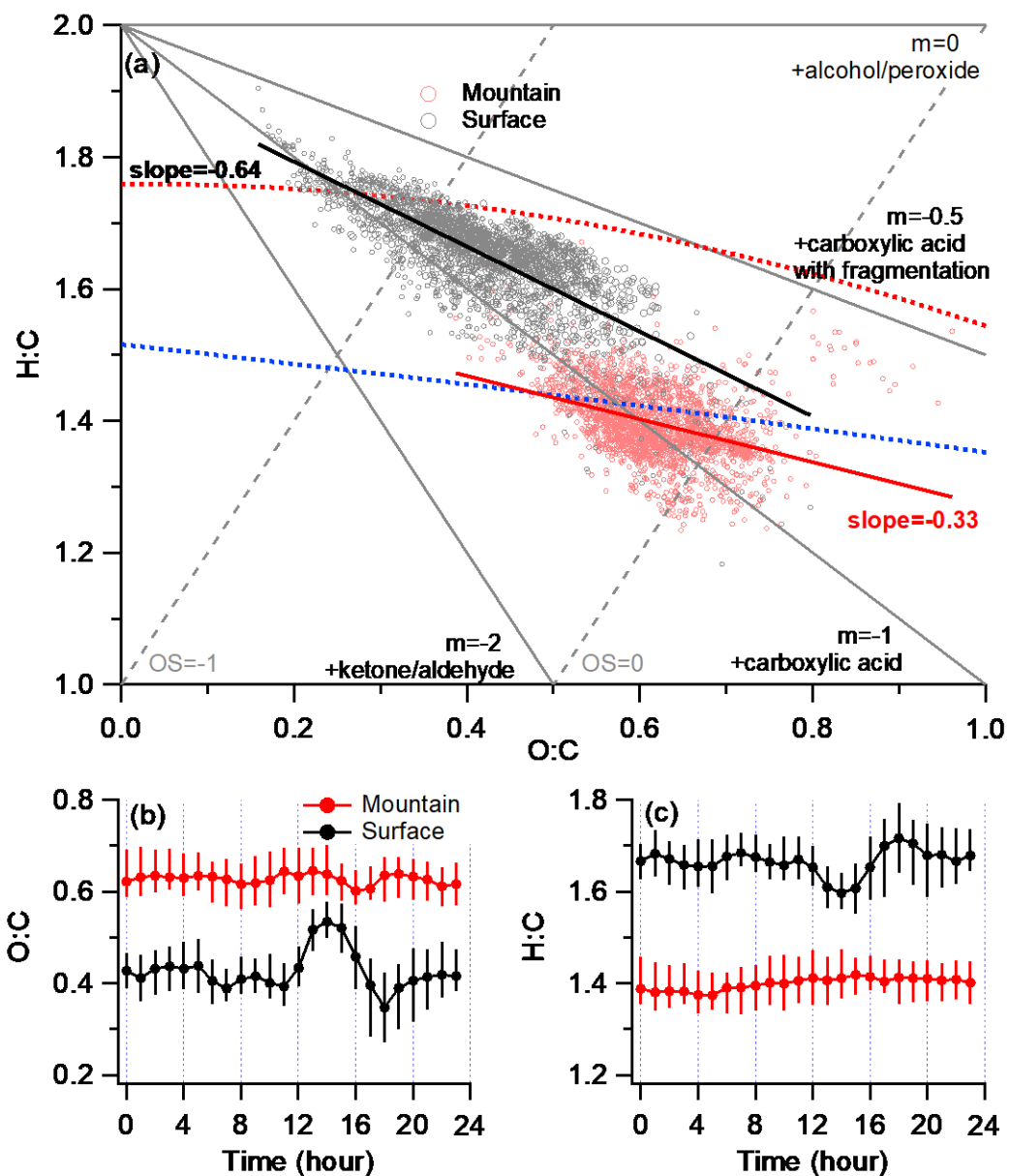


Fig. 5. Characterization of elemental ratios at both surface and mountain sites, (a) The standard Van Krevelen-triangle diagram of H:C versus O:C; (b) diurnal variations of O:C; (c) diurnal variations of H:C. The grey and red circles denote the data points from the surface and mountain sites respectively.

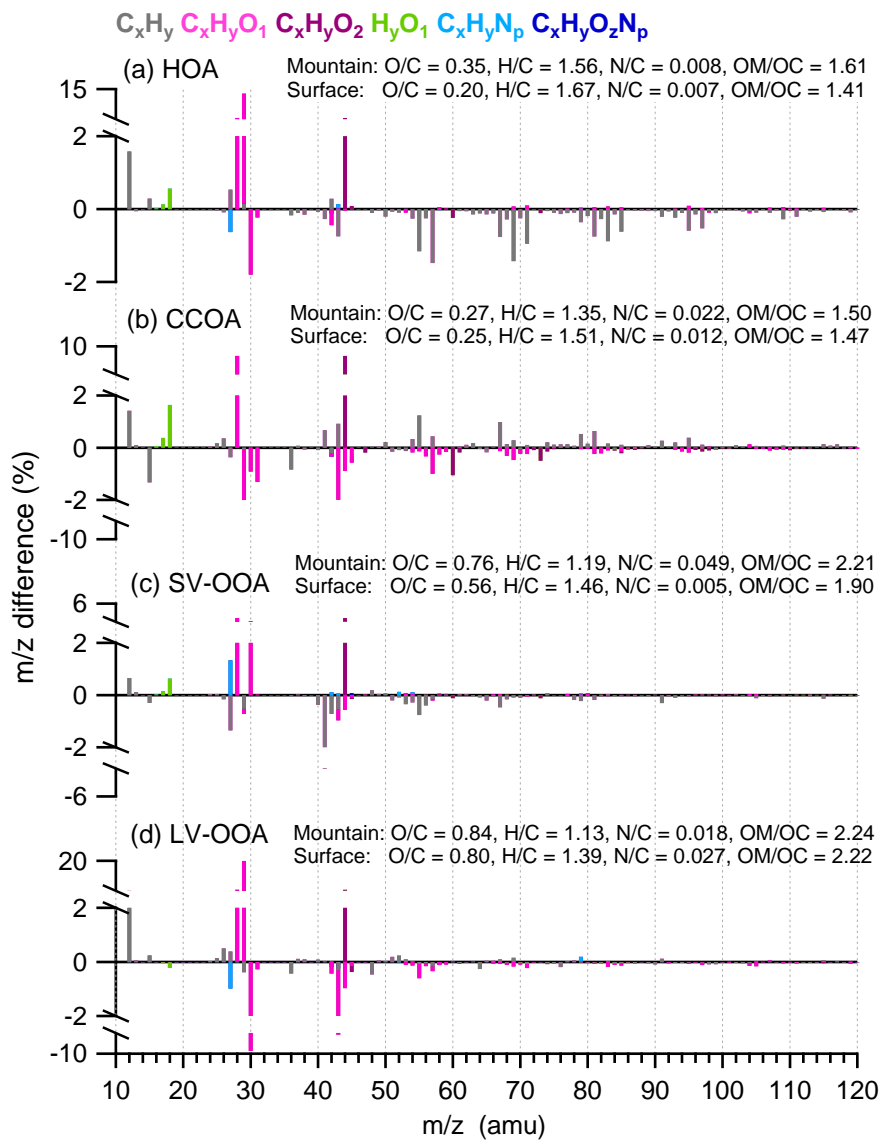


Fig. 6. Difference of mass spectra between mountain and surface sites (mountain minus surface) for (a) HOA, (b) CCOA, (c) SV-OOA, and (d) LV-OOA.